Radio Science

RESEARCH ARTICLE

10.1029/2021RS007389

Key Points:

- Qualitative insights on how the mutual impedance of cross-dipoles varies with their skew angle, common length, and separation
- The proposed phenomenological modeling approach least-squares-fits the cross-dipoles' mutual impedance values to low-dimensional models
- Despite these phenomenological models' few degrees of freedom, the proposed models successfully facilitate direction finding

Correspondence to:

Y. I. Wu,
y.i.wu@ieee.org

Citation:

Arada, G. P., Wu, Y. I., Wong, K. T., Tam, W.-Y., Khan, S., & Fulton, C. J. (2022). How two crossed dipoles' impedance varies with their non-orthogonality, length & separation. *Radio Science*, *57*, e2021RS007389. https://doi.org/10.1029/2021RS007389

Received 21 OCT 2021
Accepted 3 APR 2022

How Two Crossed Dipoles' Impedance Varies With Their Non-Orthogonality, Length & Separation

Gerald Pacaba Arada[1], Yue Ivan Wu[2], Kainam Thomas Wong[3], Wai-Yip Tam[4], Salman Khan[5], and Caleb J. Fulton[6]

[1]Department of Electronics & Communications Engineering, De La Salle University, Manila, Philippines, [2]College of Computer Science, Sichuan University, Chengdu, China, [3]School of General Engineering, Beihang University, Beijing, China, [4]Department of Electronic & Information Engineering, Hong Kong Polytechnic University, Hong Kong, China, [5]Department of Electrical Engineering, University of Engineering and Technology, Mardan, Pakistan, [6]Department of Electrical & Computer Engineering, University of Oklahoma, Norman, OK, USA

Abstract To model the electromagnetic mutual impedance between a pair of "crossed dipoles" (a.k.a. "cross dipoles") whose relative orientation is skewed (i.e., not perpendicular), this paper advances a new modeling approach – the "phenomenological" or "behavioral" approach. This new approach leads to simple models of the mutual impedance, as closed-form expressions parameterized explicitly by the dipoles' (a) skew angle, (b) separation, and (c) common length. This mathematical simplicity is unprecedented in prior models. These models' usefulness is illustrated, using direction finding as an example.

1. Introduction

A pair of crossed dipoles comprise two electric dipoles nominally orthogonal in orientation and nearly co-centered in space. Crossed dipoles have long facilitated beamforming, direction finding, and polarization estimation. Each dipole measures one distinct Cartesian component of the incident electric-field vector. A pair of crossed dipoles thus constitutes a diversely polarized array capable of distinguishing incident sources based on their polarizations, besides basing on their directions-of-arrival and frequency spectra. One pair of crossed dipoles can suffice to determine the incident electromagnetic wavefront's (bivariate) polarization and the azimuthal direction-of-arrival. For an extensive survey of the relevant literature, please refer to Yuan et al. (2012), Wong et al. (2017), Khan and Wong (2019).

If these two constituent dipoles are exactly perpendicular to each other, they would experience no electromagnetic coupling between them. (The mutual coupling would be negligible across two perpendicular dipoles, if the dipoles are fed differentially at their central feed points, due to the symmetry in both the fields and the currents/voltages of the feed structure. "Differential feeding" here refers to the signals fed to the dipoles' terminals in an opposite but equal way.) However, real-world implementations of the crossed dipoles may deviate from this idealized orthogonality, thereby resulting in mutual coupling between the two dipoles. Please refer to Figure 1, which defines the skew angle φ (i.e., the angular deviation from perpendicularity) between two identical dipoles—One on the z-axis and the other on the y'-z' plane.

A dipole pair's impedance matrix $\mathbf{Z}$ is 2×2 in size, with entries complex in value. This impedance matrix is also symmetric, centro-symmetric, and persymmetric. Hence, there exist only two distinct complex-value scalars that need to be modeled, namely $Z_{1,1} = Z_{2,2}$ and $Z_{1,2} = Z_{2,1}$. Each above complex-valued scalar may be represented by its magnitude and its complex phase. Therefore, four real-valued scalars need to be modeled. (These mutual-coupling coefficients, $\{Z_{i,j}, \forall(i,j)\}$, are independent of the incident electromagnetic field's direction-of-arrival. However, the coupled voltages and the coupled currents depend on both the mutual-coupling coefficients and the incident electromagnetic field's direction-of-arrival, as illustrated in Section 6.)

1.1. The "Phenomenological"/"Behavioral" Approach to Model Mutual Impedance

For such a pair of skewed or slanted dipoles of equal length: Previous analysis of the concerned antenna electromagnetics has led to knotty mathematical expressions for the mutual impedance: (a) As a six-page equation in Czyz (1957), (b) as an unsolved integral equation in Murray (1933), Baker and LaGrone (1962), Richmond (1970), Richmond and Geary (1975), Han and Myung (2012), Han et al. (2013), or (c) as nested summations in Richmond

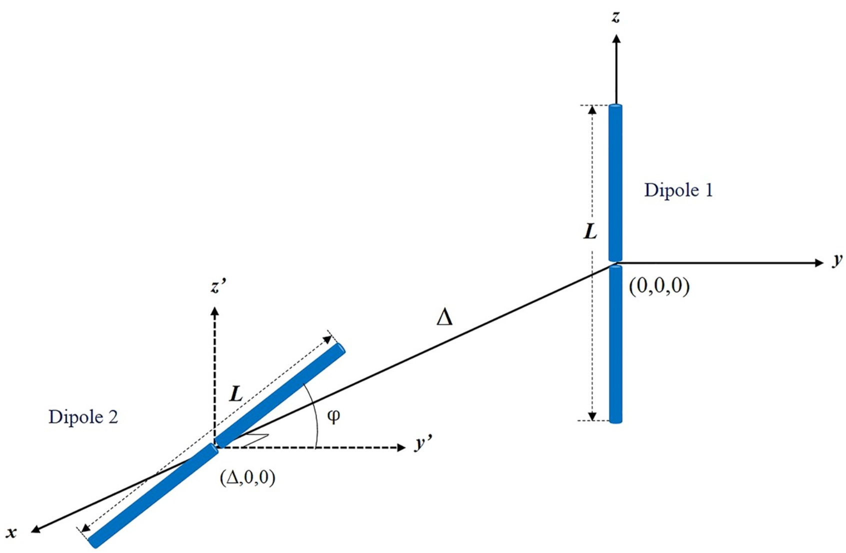

Figure 1. The spatial geometry between two cross dipoles of non-orthogonal orientation. Dipole 2 lies on the y'-z' Cartesian plane. Here, the inter-dipole separation Δ is greatly exaggerated for visual clarity.

and Geary (1970), Schmidt (1996), Han et al. (2012), (2013). These highly complicated expressions in (a–c) could hardly yield any intuitive insight on how the mutual impedance varies with the non-orthogonal skew angle (φ), the dipole length (L), and the inter-dipole gap (Δ). Indeed, Baker and LaGrone (1962), Richmond and Geary (1970), Richmond (1970), Andersen et al. (1974), Amin and Cahill (2003), (2004), Best (2011), Han and Myung (2012), Han et al. (2012) resorted to only graphic plots of the mutual impedance for only a few scenarios.

Instead, this paper will take a different approach—A "phenomenological" or "behavioral" approach that takes mutual impedance data to fit them to a low-dimensional manifold. Such a "phenomenological" or "behavioral" approach is commonplace in modeling a wireless propagation fading channel or a nonlinear amplifier's input/output relationship, though admittedly new to mutual coupling modeling. Despite the simplicity of this approach, subsequently presented results will demonstrate its success to yield simple rule-of-thumb relationships of how the mutual impedance varies with the non-orthogonal skew angle (φ), with the wavelength-normalized dipole length $\left(\frac{L}{\lambda}\right)$, and with the wavelength-normalized inter-dipole gap $\left(\frac{\Delta}{\lambda}\right)$.

1.2. "Method of Moment" Simulations of Mutual Impedance

The skewed dipole-pair's mutual impedance is approximated below by numerical simulations to solve the Maxwell equations, via the "method of moments" (MoM), a.k.a. the "boundary element method" (BEM). This "method of moments" is known for its reliable solution for the unknown current distributions on wire antennas. This simulation fidelity is critical here, because *near*-field mutual coupling is induced by a smooth current distribution on the dipoles and by rapid changes of the current distribution near the feed point, unlike *far*-zone radiation pattern evaluation. The specific software used is the "EMCoS Antenna VLab". The "EMCoS Antenna VLab" simulations are conducted by simultaneously exciting each dipole with its own voltage source and while connecting each dipole to its own load. These "method of moments" results will be least-squares fit to mathematically simple phenomenological/behavioral models in Sections 2 to 5.

In all subsequently presented results: each dipole's diameter is maintained at $\frac{\lambda}{5\times10^4}$; each dipole's feeding gap equals $\frac{\lambda}{50}$; and the voltage source's internal impedance is always matched to a half-wavelength dipole, regardless of the actual value of $\frac{L}{\lambda}$.

The dipole-pair would be simulated for these ranges of values:

1. The skewed angle $\varphi \in [1°, 45°]$.
2. Each dipole's electric length $\frac{L}{\lambda} \in [0.1, 1.0]$.
3. Spatial separation between the two dipoles' feeding centers $\frac{\Delta}{\lambda} \in [0.01, 2.0]$.

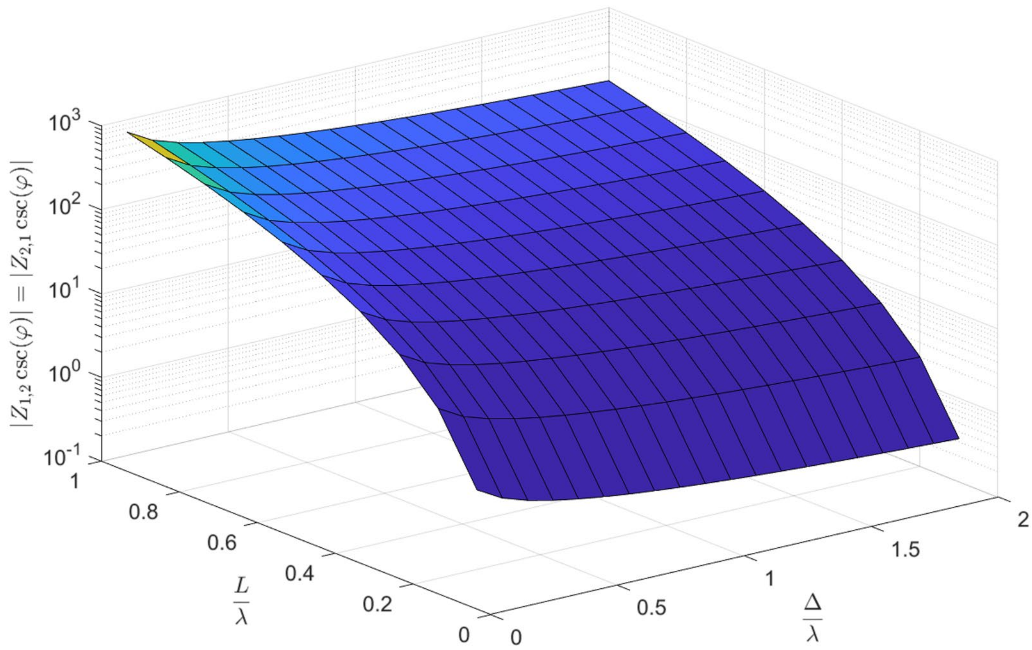

Figure 2. How $|Z_{1,2}\csc(\varphi)| = |Z_{2,1}\csc(\varphi)|$ of Equation 1 varies with $\frac{\Delta}{\lambda}$ and $\frac{L}{\lambda}$.

Any model's goodness-of-fit to any data set may be measured by the "coefficient of determination", $R^2 \in [0, 1]$. This R^2 value indicates what fraction of the data is predicted by the mathematical model.

Furthermore, the fewer the degrees-of-freedom (DoF) in the model, the better the model would be.

2. Phenomenological Model Fitting of the Mutual Impedance's Magnitude $|Z_{1,2}| = |Z_{2,1}|$

For the mutual impedance magnitude, the proposed phenomenological model is

$$|Z_{1,2}| = |Z_{2,1}| \approx 10^{a_1}\left(\frac{\Delta}{\lambda}\right)^{-a_2}\left(\frac{L}{\lambda}\right)^{a_3}|\sin(\varphi)|, \tag{1}$$

where $a_1 := 2.3018$, $a_2 := 0.5564$, $a_3 := 2.6230$. The goodness-of-fit R^2 equals 0.8599, that is, 86% of the variation in the VLab-simulated data set of $|Z_{1,2}|$ and $|Z_{2,1}|$ cannot be predicted by the phenomenological model of Equation 1. Please see Figure 2.

A more elegant expression may be obtained by rounding the above three coefficients' values to $a_1 = 23/10 = \log_{10}(200)$, $a_2 = \frac{5}{9}$, $a_3 = \sqrt{7}$, resulting in an R^2 of 0.8598. The R^2 values are evaluated on the logarithmic entities of

$$\log_{10}|Z_{1,2}| = \log_{10}|Z_{2,1}| \approx a_1 - a_2\log_{10}\left|\frac{\Delta}{\lambda}\right| + a_3\log_{10}\left|\frac{L}{\lambda}\right| + \log_{10}|\sin(\varphi)| \tag{2}$$

instead of $|Z_{1,2}| = |Z_{2,1}|$ itself as in Equation 1. This is because $|Z_{1,2}| = |Z_{2,1}|$ has values across several orders of magnitude. Hence, the latter would overweight those support subregions of $\left\{\varphi, \frac{L}{\lambda}, \frac{\Delta}{\lambda}\right\}$ where $|Z_{1,2}| = |Z_{2,1}|$ is very large, thereby poorly fitting other subregions of $\left\{\varphi, \frac{L}{\lambda}, \frac{\Delta}{\lambda}\right\}$ where $|Z_{1,2}| = |Z_{2,1}|$ is small. Specifically, the would-be-underweighted support subregion is where $\frac{L}{\lambda}$ increases toward unity and where $\frac{\Delta}{\lambda}$ decreases toward zero.

The negative power of $\frac{\Delta}{\lambda}$ in Equation 1 indicates that $|Z_{1,2}| = |Z_{2,1}|$ decreases monotonically with an increasing inter-dipole separation $\frac{\Delta}{\lambda}$. Indeed, as $\frac{\Delta}{\lambda} \to \infty$, the model gives $|Z_{1,2}| = |Z_{2,1}| \to 0$. This trend is reasonable in terms of electromagnetics, because $Z_{1,2} = Z_{2,1}$ is proportional to the induced electric field, whose magnitude is inversely related to the distance between the driving dipole and the induced dipole.

That $|Z_{1,2}| = |Z_{2,1}|$ increases with $\frac{L}{\lambda}$ is reasonable: As $\frac{L}{\lambda}$ lengthens, the driving dipole's re-radiation strengthens. Hence, the coupled dipole's induced voltage rises, thereby increasing $|Z_{1,2}| = |Z_{2,1}|$.

The non-negative factor, $|\sin\varphi|$, in the model of Equation 1 suggests that $|Z_{1,2}| = |Z_{2,1}|$ would increase monotonically, as the two dipoles become less perpendicular with each other. This is reasonable in terms of electromagnetics: This $|\sin\varphi|$ factor arises from the projection of the driving dipole's electric field on the induced dipole, which is skewed from the former dipole by a rotational angle of φ. As the skew angle $|\varphi|$ increases from 0 toward 90°, the two dipoles would become more parallel, hence more mutual coupling between them. Under the special case where the two dipoles are perfectly orthogonal (i.e., $\varphi = 0$), $|Z_{1,2}| = |Z_{2,1}| = 0$ in Equation 1, as expected.

In more antennas-electromagnetics details: Consider the primary dipole's re-radiated electric field, using the notation of $\left\{\vec{\mathbf{E}}_r, \vec{\mathbf{E}}_\phi, \vec{\mathbf{E}}_\theta\right\}$, which is standard in the antenna-electromagnetics literature (e.g., please see Figure 4. 1 of (Balanis, 2005)). Both $\vec{\mathbf{E}}_r$ and $\vec{\mathbf{E}}_\phi$ are effectively orthogonal to the secondary dipole's feeding gap regardless of the inter-dipole skew angle of φ, hence have no/little significance on the mutual impedance. Only $\vec{\mathbf{E}}_\theta$ has any noteworthy effect upon the secondary dipole. This $\vec{\mathbf{E}}_\theta$ has a complex-valued amplitude related to the polar angle of θ and r as follows (according to pp. 133–136 of (Balanis, 2005)): $K\sin(\theta)\frac{\lambda}{2\pi r}\left[1 - j\frac{\lambda}{2\pi r} + \left(\frac{\lambda}{2\pi r}\right)^2\right]\exp\left(-j\frac{2\pi r}{\lambda}\right)$, where K denotes a constant scalar independent of both θ and r. In this discussion: $\theta \approx \varphi$ (i.e., the inter-dipole skew angle), and $r = \Delta$ (i.e., the inter-dipole gap). For almost all practical dipole-pairs of interest: $\frac{\Delta}{\lambda} \ll \frac{1}{2\pi}$, thereby approximating the above expression to

$$K\sin(\varphi)\left(\frac{\lambda}{2\pi\Delta}\right)^3 \exp\left(-j\frac{2\pi\Delta}{\lambda}\right). \tag{3}$$

The above $\sin(\varphi)$ factor appears in Equation 1.

3. Phenomenological Model Fitting of the Mutual Impedance's Complex-Phase $\angle Z_{1,2} = \angle Z_{2,1}$

For the mutual impedance's phase, the proposed phenomenological model is.

$$\angle Z_{1,2} = \angle Z_{2,1} \approx b_1\frac{\Delta}{\lambda} + b_2\frac{L}{\lambda} + b_3, \tag{4}$$

$$\begin{aligned} b_1 &:= -5.5920, \\ b_2 &:= 0.5048\pi, \\ b_3 &:= -0.2952. \end{aligned} \tag{5}$$

The goodness-of-fit R^2 equals 0.9655, that is, only 4% of the variation in the VLab-simulated data set of $\angle Z_{1,2}$ and $\angle Z_{2,1}$ cannot be predicted by the phenomenological model of Equation 4.

A more elegant expression may be obtained by rounding the above three coefficients' values to $b_1 = -50/9$, $b_2 = \frac{\pi}{2}$, $b_3 = -\log_{10}(2)$, resulting in an R^2 of 0.9654.

This model of $\angle Z_{1,2} = \angle Z_{2,1}$ decreases linearly with the inter-dipole separation $\frac{\Delta}{\lambda}$. This is reasonable in terms of antenna electromagnetics: As the radiation propagates outward from the driving dipole, its phase will change linearly with the distance (Δ) traversed between the two dipoles, as evidenced by Equation 3 whose complex phase varies linearly with Δ.

This model of $\angle Z_{1,2} = \angle Z_{2,1}$ is independent of the inter-dipole skew angle φ, in accordance with the VLab data. This is reasonable in terms of antenna electromagnetics: The phase $\angle Z_{1,2} = \angle Z_{2,1}$ depends on the distance traveled by the driving dipole's radiated electric field to the induced dipole. If the induced dipole is rotated with respect to its feed center, the feed-center to feed-center separation would remain the same. Hence, the inter-dipole skew angle φ has no effect on $\angle Z_{1,2}$.

10.1029/2021RS007389

This model of $\angle Z_{1,2} = \angle Z_{2,1}$ increases linearly with the dipoles' electric length $\frac{L}{\lambda}$. This is reasonable in terms of dipole electromagnetics: The radiation is emitted from the driving dipole along that dipole's entire length, and is received by the induced dipole along the induced dipole's entire length. The inter-dipole separation thus involves the distance from any point on the driving dipole to any point on the induced dipole. Such point-to-point distances have an average that increases linearly with the two dipoles' length. Hence, the phase would change also linearly with $\frac{L}{\lambda}$.

4. Phenomenological Model Fitting of the Self-Impedance's Magnitude $|Z_{1,1}| = |Z_{2,2}|$

For the self-impedance magnitude, the proposed phenomenological model is

$$\begin{aligned} |Z_{1,1}| &= |Z_{2,2}| \\ &\approx \overbrace{\left| p_1 + p_2 \cos\left(p_3 \frac{\Delta}{\lambda} + p_4\right) e^{-p_5 \frac{\Delta}{\lambda}} \sin^2(\varphi) \right|}^{P_1\left(\frac{\Delta}{\lambda}, \varphi\right) :=} \overbrace{\left[\left(\frac{L}{\lambda} - p_6\right)^2 + p_7 \right]}^{P_2\left(\frac{L}{\lambda}\right) :=}, \end{aligned} \tag{6}$$

where p1 ≔ 20415.4041, p2 ≔ 98.3895, p3 ≔ 4.0412π, p4 ≔ 3.4539π, p5 ≔ 0.2782, p6 ≔ 0.4838, p7 ≔ 0.0057.

The goodness-of-fit R^2 equals 0.9808, that is, only 2% of the variation in the VLab-simulated datasets of $|Z_{1,1}|$ and $|Z_{2,2}|$ cannot be predicted by the phenomenological model of Equation 6. The R^2 is evaluated on the logarithmic entities of

$$\begin{aligned} \log_{10}|Z_{1,1}| &= \log_{10}|Z_{2,2}| \\ &\approx \log_{10}\left| p_1 + p_2 \cos\left(p_3 \frac{\Delta}{\lambda} + p_4\right) e^{-p_5 \frac{\Delta}{\lambda}} \sin^2(\varphi) \right| + \log_{10}\left| \left(\frac{L}{\lambda} - p_6\right)^2 + p_7 \right|, \end{aligned} \tag{7}$$

instead of $|Z_{1,1}| = |Z_{2,2}|$ directly from Equation 6. This is because $|Z_{1,1}| = |Z_{2,2}|$ takes on values spanning several orders of magnitude. Hence, any R^2 computation based on Equation 6 would overweight those support subregions of $\left\{\varphi, \frac{L}{\lambda}, \frac{\Delta}{\lambda}\right\}$ where $|Z_{1,1}| = |Z_{2,2}|$ is very large, thereby poorly fitting other subregions of $\left\{\varphi, \frac{L}{\lambda}, \frac{\Delta}{\lambda}\right\}$ where $|Z_{1,1}| = |Z_{2,2}|$ is small. More explicitly, the would-be-overweighted subregion is where $\frac{L}{\lambda}$ increases toward unity and where $\frac{\Delta}{\lambda}$ decreases toward zero.

A more elegant expression may be obtained by rounding the above coefficients' values to $p_1 = 20000$, $p_2 = 10\pi^2$, $p_3 = 4\pi$, $p_4 = \frac{5}{9}\pi$, $p_5 = e$, $p_6 = \frac{97}{200}$, $p_7 = \frac{6}{1000}$, resulting in an R^2 of 0.9805.

The two dipoles' separation $\frac{\Delta}{\lambda}$ affects $|Z_{1,1}| = |Z_{2,2}|$ only through $P_1\left(\frac{\Delta}{\lambda}\right)$. Please see Figure 3. If the two dipoles are very far apart (i.e., as $\frac{\Delta}{\lambda} \to \infty$): $P_1\left(\frac{\Delta}{\lambda}\right) \to p_1$; and the second term inside $|\cdot|$ approaches zero.

The two dipoles' skew angle φ affects $|Z_{1,1}| = |Z_{2,2}|$ only through $\sin^2(\varphi)$. This $\sin^2(\varphi)$ multiplicative factor may be interpreted to arise from the round-trip propagation of the radiated electric field, from the excited dipole, to the induced dipole, then back to the excited dipole. Recalling that these two dipoles are skewed with respect to each other by φ, this induced electric field (as mentioned in Section 2) is proportional to $|\sin(\varphi)|$ for each one-way propagation. When the two dipoles are orthogonal (i.e., $\varphi = 0$), the second term inside $|\cdot|$ equals zero.

The two preceding paragraphs point out that the second term inside $|\cdot|$ approaches zero, if and only if either the two dipoles are orthogonal (i.e., $\varphi = 0$) or very far apart $\left(\frac{\Delta}{\lambda} \to \infty\right)$, such that the driving dipole would become effectively isolated from the induced dipole. Hence, that second term could be interpreted to correspond to re-radiation from the induced dipole. In other words, the driving dipole's self-impedance $Z_{1,1}$ is (a) partly due to the driving dipole's isolated self-impedance, and (b) partly due to the electric field induced back to the driving dipole by the induced dipole. Effect (a), however, is at least $\frac{p_1}{p_2} \approx 207$ times more significant than effect (b). This is reasonable in terms of antenna electromagnetics: The inter-dipole coupling's aforementioned round-trip effect

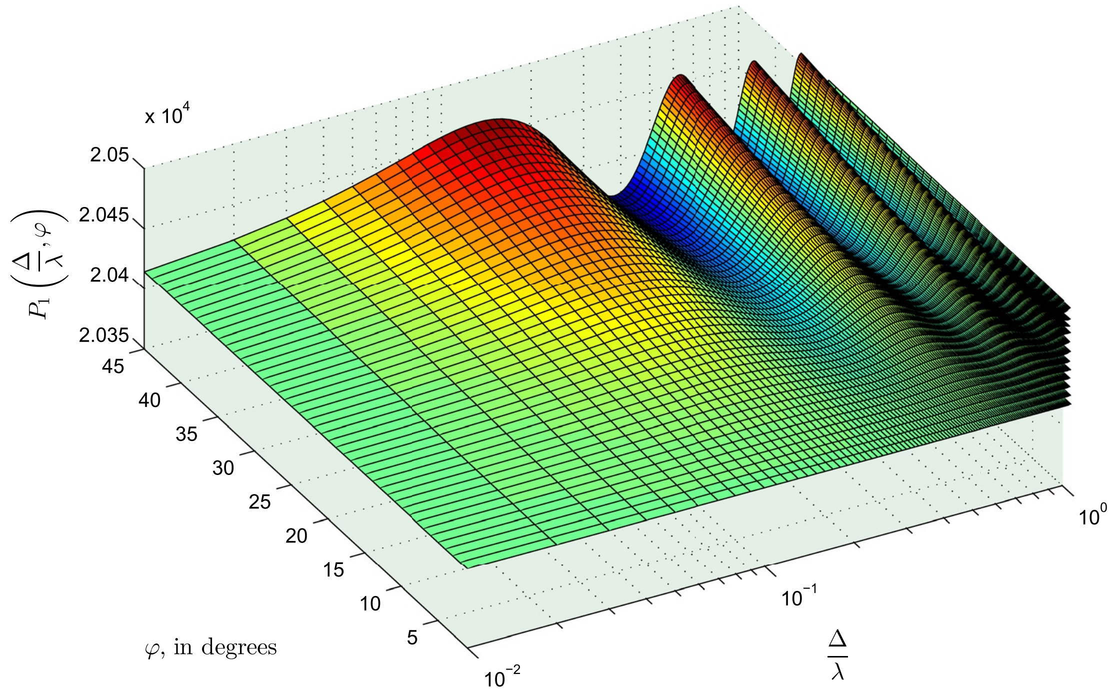

Figure 3. How $P_1\left(\frac{\Delta}{\lambda}, \varphi\right)$ varies with $\frac{\Delta}{\lambda}$ and φ.

(i.e., round trip from the driving dipole to the induced dipole, then back to the driving dipole) would render effect (b) to be much smaller than the driving dipole's own isolated self-impedance.

When the two dipoles are either very widely separated or orthogonally oriented, the model in Equation 6 would degenerate to the mathematical form of $p_1 P_2\left(\frac{L}{\lambda}\right)$, which is a reasonable representation of an isolated dipole's self-impedance. The dipoles' length $\frac{L}{\lambda}$ affects $|Z_{1,1}| = |Z_{2,2}|$ only through the multiplicative factor $P_2\left(\frac{L}{\lambda}\right)$.

5. Phenomenological Model Fitting of the Self-Impedance's Complex Phase $\angle Z_{1,1} = \angle Z_{2,2}$

For the self-impedance's phase, the proposed phenomenological model is

$$\angle Z_{1,1} = \angle Z_{2,2} \approx \left\{ q_1 + \overbrace{q_2 \sin\left(q_3 \frac{\Delta}{\lambda}\right) e^{-q_4 \frac{\Delta}{\lambda}}}^{Q\left(\frac{\Delta}{\lambda}\right) :=} \right\} \sin\left(q_5 \frac{L}{\lambda}\right), \tag{8}$$

where q1 ≔ 1.7648, q2 ≔ 0.0103, q3 ≔ 0.7091π, q4 ≔ 5.0565, q5 ≔ −2.0758π.

The goodness-of-fit R^2 equals 0.9018; that is, over 90% of the variation in the VLab-simulated data set of $\angle Z_{1,1}$ and $\angle Z_{2,2}$ can be predicted by phenomenological model of Equation 8.

Like $|Z_{1,1}| = |Z_{2,2}|$ in Section 4, the phenomenological model here for $\angle Z_{1,1} = \angle Z_{2,2}$ has two terms inside the curly brackets. The first term corresponds to each dipole's isolated self-impedance, whereas the second term arises due to the re-radiation from the induced dipole back to the driving dipole. Figure 4 plots $Q\left(\frac{\Delta}{\lambda}\right)$ versus $\frac{\Delta}{\lambda}$. The

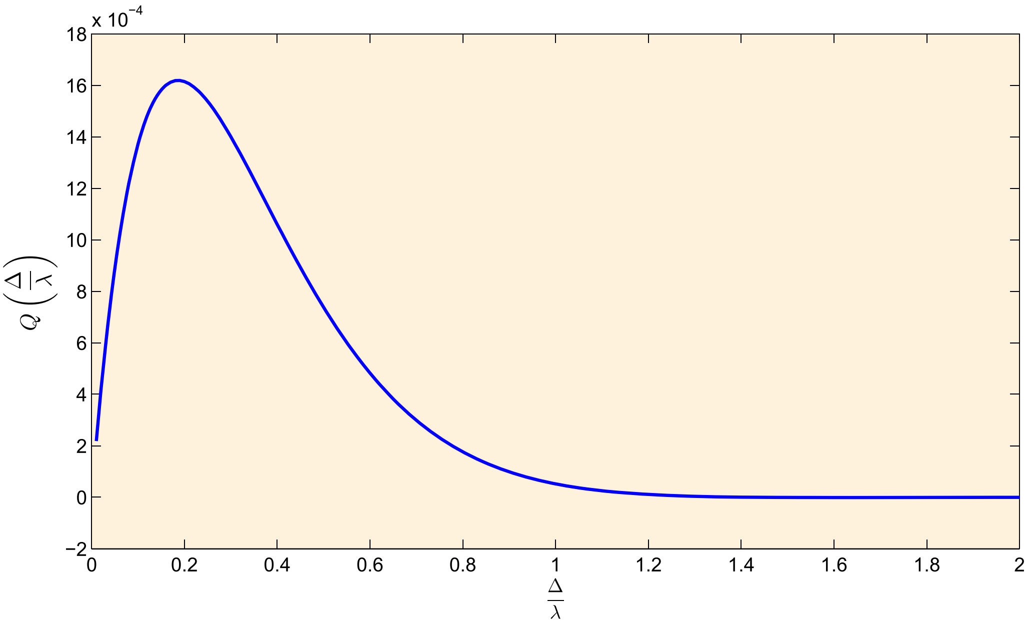

Figure 4. How $Q\left(\frac{\Delta}{\lambda}\right)$ varies with $\frac{\Delta}{\lambda}$.

first term dominates the second term (by a ratio of $\frac{q_1}{q_2} \approx 171$ multiples), as would be expected and as explained in Section 4.

To simplify Equation 8, remove $Q(\cdot)$ from Equation 8 to give

$$\angle Z_{1,1} = \angle Z_{2,2} \approx q_1 \sin\left(q_2 \frac{L}{\lambda}\right). \tag{9}$$

This bivariate model still gives $R^2 = 0.8800$ at $q_1 = \sqrt{3}$ and $q_2 = -2\pi$.

Like $\angle Z_{1,2} = \angle Z_{2,1}$ in Section 3, the phenomenological model here for $\angle Z_{1,1} = \angle Z_{2,2}$ is independent of φ, for reasons already explained in Section 3.

6. Application to Direction Finding

To demonstrate the usefulness of the new phenomenological models in Equations 1, 4, 6 and 8—These models are utilized below for the estimation of an incident source's azimuth-elevation direction-of-arrival (DOA).

6.1. The Skewed Dipole-Pair's Electromagnetic Measurement Model

Please recall the skewed dipoles' spatial geometry shown in Figure 1: The first dipole is aligned along the z-axis and is centered at the Cartesian origin. The second dipole lies on the x-y plane and is centered at the Cartesian point of $(\Delta, 0, 0)$. The second dipole's location incurs a spatial phase factor of $e^{j2\pi\frac{\Delta}{\lambda}\sin(\theta)\cos(\phi)}$, where $\theta \in [0°, 180°]$ symbolizes the incident source's polar angle of arrival, and $\phi \in [0°, 360°)$ denotes the azimuth angle of arrival measured from the positive x-axis. The second dipole's skewed orientation on the y'-z' plane implies that its voltage is affected by the incident electromagnetic wave's y-component and z-component.

If these dipoles have an electrical length $\frac{L}{\lambda} > \frac{1}{10}$, the crossed-dipoles would have this 2×1 array manifold Wong et al. (2017):

10.1029/2021RS007389

$$\begin{aligned}\mathbf{a}_{\text{pair}} &= \mathbf{C}\begin{bmatrix} 1 & 0 \\ 0 & e^{j2\pi\frac{\Delta}{\lambda}\sin(\theta)\cos(\phi)} \end{bmatrix}\begin{bmatrix} 0 & 1 \\ \cos(\varphi) & \sin(\varphi) \end{bmatrix} \\ &\quad \left\{\begin{bmatrix} -\sin(\phi) & 0 \\ \cos(\theta)\sin(\phi) & \cos(\phi) \end{bmatrix}\begin{bmatrix} e^{j\eta}\sin\gamma \\ \cos\gamma \end{bmatrix} \circ \begin{bmatrix} \ell_\theta \\ \ell_\psi \end{bmatrix} \circ \begin{bmatrix} \csc(\theta) \\ \csc(\psi) \end{bmatrix}\right\},\end{aligned} \tag{10}$$

with the "effective lengths" of

$$\begin{aligned}\ell_\theta &= -\frac{\lambda}{\pi}\frac{1}{\sin\left(\pi\frac{L}{\lambda}\right)}\frac{\cos\left(\pi\frac{L}{\lambda}\cos(\theta)\right)-\cos\left(\pi\frac{L}{\lambda}\right)}{\sin(\theta)}, \\ \ell_\psi &= -\frac{\lambda}{\pi}\frac{1}{\sin\left(\pi\frac{L}{\lambda}\right)}\frac{\cos\left(\pi\frac{L}{\lambda}\cos(\psi)\right)-\cos\left(\pi\frac{L}{\lambda}\right)}{\sin(\psi)},\end{aligned}$$

and

$$\begin{aligned}\cos(\psi) &= \sin(\theta)\sin(\phi)\cos(\varphi)+\cos(\theta)\sin(\varphi), \\ \sin(\psi) &= \left(\sin^2(\theta)\sin^2(\varphi)+\cos^2(\theta)\cos^2(\varphi)\right. \\ &\quad \left. +\ \sin^2(\theta)\cos^2(\phi)\cos^2(\varphi) - \frac{1}{2}\sin(2\theta)\sin(2\varphi)\sin(\phi)\right)^{\frac{1}{2}}\end{aligned}$$

In the above, $\gamma \in \left[0, \frac{\pi}{2}\right]$ denotes the auxiliary polarization angle, $\eta \in [-\pi, \pi]$ refers to the polarization phase difference, ψ refers to the angle made between the slanted dipole and the unit vector along the direction of propagation, and $\circ$ denotes element-wise multiplication. Furthermore, $\mathbf{C}$ symbolizes the dipoles' 2×2 electromagnetic coupling matrix, which is related to the impedance matrix $\mathbf{Z}$ as follows [Gupta and Ksienski (1983), Yang and Ruan (1993), Svantesson (1998), (1999), Al-Kabi et al. (2006), Huang et al. (2006a), (2006b), Weber and Huang (2012), Akkar et al. (2013)]:

$$\mathbf{C} = \left(\frac{\mathbf{Z}}{Z_0} + \mathbf{I}\right)^{-1}.$$

The subsequent direction-finding study would consider three cases:

1. The actual impedance matrix is *exactly known* to the direction-of-arrival estimation algorithm, a priori. Here, $\mathbf{Z}$ would equal the VLab output values. This case corresponds to the dotted black curve on the subsequent graphs.
2. The actual impedance matrix is *un*known to the direction-of-arrival estimation algorithm. Instead, the phenomenological models of Equation 1, 4, 6 and 8 are used to form $\mathbf{Z}$ for use in the estimation algorithm. This case corresponds to the solid red curve on the subsequent graphs.
3. Mutual coupling is presumed erroneously by the direction-of-arrival estimation algorithm to be nonexistent. Here, $\mathbf{Z}$ equals a 2×2 matrix of all zeros. This case corresponds to the dash-dot blue curve on the subsequent graphs.

6.2. The Data's Statistical Model

Let the receiver be equipped with a square array of four identical pairs of skewed-dipoles, each of which is as described above in Section 6.1. This square array's each side is 7λ in length—A separation long enough to render any inter-pair coupling to be negligible. This array's 8×1 array manifold may be represented as

$$\mathbf{a}_{\text{array}}(\theta,\phi,\gamma,\eta)=\mathbf{a}_{\text{pair}}\otimes\begin{bmatrix}\exp\{j7\pi\sin(\theta)[+\sin(\phi)+\cos(\phi)]\}\\ \exp\{j7\pi\sin(\theta)[+\sin(\phi)-\cos(\phi)]\}\\ \exp\{j7\pi\sin(\theta)[-\sin(\phi)+\cos(\phi)]\}\\ \exp\{j7\pi\sin(\theta)[-\sin(\phi)-\cos(\phi)]\}\end{bmatrix},\tag{11}$$

where $\otimes$ symbolizes the Kronecker product.

To focus on the electromagnetic coupling among the dipoles and on the proposed phenomenological models, an admittedly simple statistical model will be used below for the incident signal and the noise. Suppose a pure tone signal $s(t)=\exp[j(\omega t+\varphi)]$ impinges on the aforementioned receiver. At the mth time-instant, the collected data may be modeled as an 8×1 vector of

$$\mathbf{x}(m)=\frac{\mathbf{a}_{\text{array}}(\theta,\phi,\gamma,\eta)}{\|\mathbf{a}_{\text{array}}(\theta,\phi,\gamma,\eta)\|}s(m)+\mathbf{n}(m).\tag{12}$$

In the above, $\|\cdot\|$ represents the Frobenius norm, and $\mathbf{n}(m)$ denotes an 8×1 vector of additive noise, modeled here as Gaussian, zero in mean, statistically uncorrelated over the time-instants and uncorrelated across all eight dipoles. The normalization in Equation 12 by $\|\mathbf{a}_{\text{array}}(\theta,\phi,\gamma,\eta)\|$ is for a fair comparison across the three impedance cases (A)–(C) in Section 6.1.

With M number of time samples, form an $8\times M$ data matrix of

$$\mathbf{X}:=[\mathbf{x}(1),\mathbf{x}(2),\ldots,\mathbf{x}(M)],$$

Each subsequent Monte Carlo simulation has $M=50$ number of time-samples.

6.3. *MUSIC*-Based Direction Finding

"Direction finding" aims to estimate the incident source's incident direction-of-arrival (θ,ϕ), based on the observations of $\mathbf{X}$.

The estimation algorithm has prior knowledge of the numerical values of $\frac{L}{\lambda},\frac{\Delta}{\lambda},\varphi$. All subsequent simulations will use these numerical settings: $\varphi=45°$, $\frac{L}{\lambda}=\frac{1}{2}$, and $\frac{\Delta}{\lambda}=\frac{1}{100}$.

MUSIC Schmidt (1996) is a popular parameter estimator, based on a eigen-decomposition of the data correlation matrix, $\mathbf{R}:=\mathbf{X}^H\mathbf{X}$. Eigen-decompose this 8×8 matrix to obtain its null space, spanned by the columns of $\mathbf{U}_{\text{null}}$. That is,

$$\mathbf{R}=[\mathbf{U}_s,\mathbf{U}_n]^H\,\mathbf{\Lambda}\,[\mathbf{U}_s,\mathbf{U}_n]\,.$$

Then, the direction-of-arrival estimates and the polarization estimates are given by

$$\left(\hat{\theta},\hat{\phi},\hat{\gamma},\hat{\eta}\right):=\underset{(\theta,\phi,\gamma,\eta)}{\arg\max}\frac{1}{\|\mathbf{U}_n^H\mathbf{a}_{\text{array}}(\theta,\phi,\gamma,\eta)\mathbf{C}\|^2},\tag{13}$$

where $\|\cdot\|$ represents the Frobenius norm of the entity inside.

Figures 5 and 6 show the estimation root-mean-square error (RMSE) of $\hat{\theta}$ and $\hat{\phi}$, versus the SNR, for the three cases (A)–(C) in Section 6.1. Each icon in Figures 5 and 6 represents 100 independent Monte Carlo trials. These figures verify the usefulness of the proposed phenomenological models—That these models offer estimation precisions almost as good as if the exact impedance were known, whereas ignoring mutual coupling causes a degradation that can be several orders of magnitude.

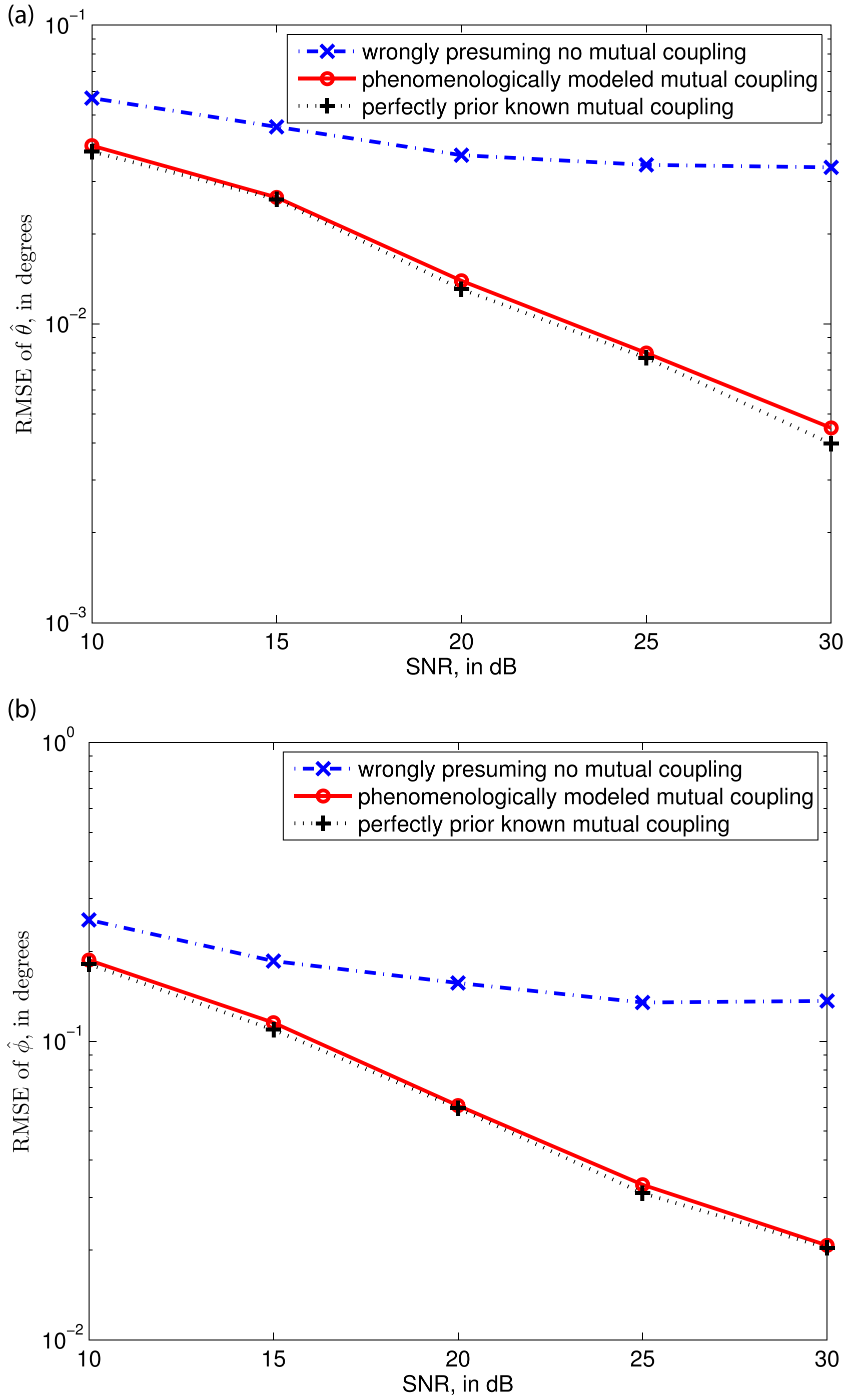

Figure 5. Monte Carlo simulations showing the proposed phenomenological models allow the mutual coupling to be a priori unknown but still facilitate direction finding to perform as if the mutual coupling well prior known. Here, $\frac{L}{\lambda} = \frac{1}{2}$, $\frac{\Delta}{\lambda} = 0.02$, $\varphi = 45°$, $\theta = 12°$, $\phi = 48°$, $\gamma = 16°$, and $\eta = 52°$.

7. Conclusion

The open literature's earlier analysis of dipole electromagnetics has produced equations of such intractable complexity, that little intuitive rule-of-thumb qualitative insights are obtained on how the mutual impedance magnitude of a pair of skewed co-centered cross-dipoles of equal length would vary with the dipoles' skew angle,

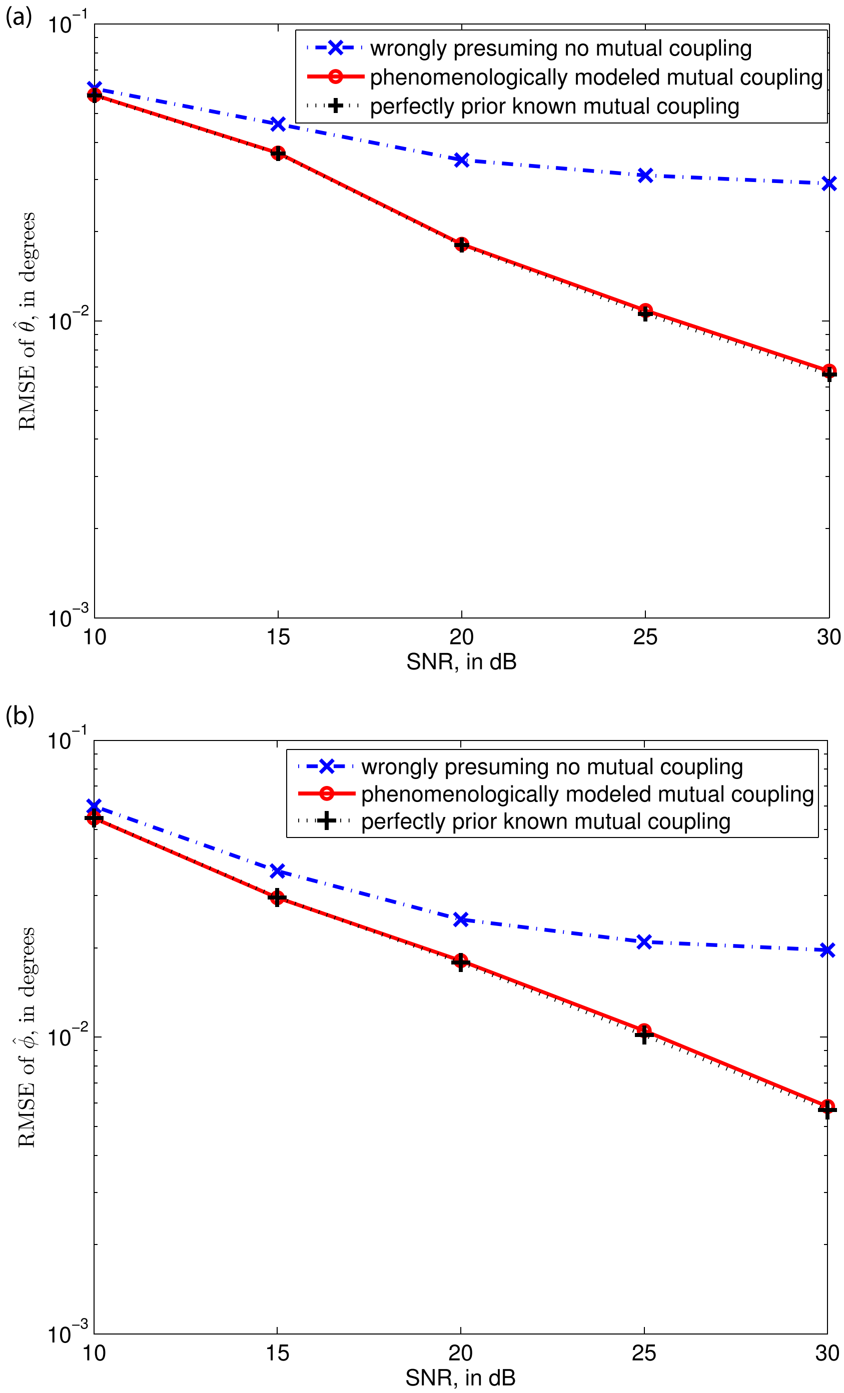

Figure 6. Monte Carlo simulations showing the proposed phenomenological models allow the mutual coupling to be a priori unknown but still facilitate direction finding to perform as if the mutual coupling well prior known. Here, $\frac{L}{\lambda} = \frac{3}{4}$, $\frac{\Delta}{\lambda} = 0.04$, $\varphi = 45°$, $\theta = 48°$, $\phi = 56°$, $\gamma = 14°$, and $\eta = -14°$.

the dipoles' common length, and the dipoles' separation. This work takes a "phenomenological" or "behavioral" approach of modeling, to least-squares-fit mutual impedance values to low-dimensional models. These new models are found useful in direction finding, despite these models' few degrees of freedom—Monte Carlo simulations illustrate how the proposed phenomenological models allow the mutual coupling to be a priori unknown but still facilitate direction finding to perform as if the mutual coupling well prior known.

Data Availability Statement

No data was created or used in this manuscript.

Acknowledgments
This work is supported by grant # 62071018 from the National Natural Science Foundation of China. The authors would like to thank Professor Danilo Erricolo, Professor Wen-Jiao Liao, and Professor Malcolm Ng for discussions on background issues related to dipoles and mutual coupling. The authors would like to thank Professor Tsair-Chuan Lin for discussions on background issues related to R^2.

References

Akkar, S., Harabi, F., & Garsallah, A. (2013). Directions of arrival estimation with planar antenna arrays in the presence of mutual coupling. *International Journal of Electronics*, *100*(6), 818–836. https://doi.org/10.1080/00207217.2012.720956

Al-Kabi, A., Bialkowski, M. E., & Homer, J. (2006). Performance comparison between uniformly and nonuniformly spaced adaptive antennas with respect to tolerance to pointing errors. *Microwave and Optical Technology Letters*, *48*(11). https://doi.org/10.1002/mop.21904

Amin, M., & Cahill, R. (2003). Mutual coupling effects between coplanar crossed skew dipoles. In *High frequency postgraduate student colloquium*.

Amin, M., & Cahill, R. (2004). Mutual impedance between two dipole antennas fed by single source. *Microwave and Optical Technology Letters*, *42*(3), 187–189. https://doi.org/10.1002/mop.20247

Andersen, J. B., Lessow, H. A., & Schjaer-Jacobsen, H. (1974). Coupling between minimum scattering antennas. *IEEE Transactions on Antennas and Propagation*, *22*(6), 832–835. https://doi.org/10.1109/tap.1974.1140912

Baker, H. C., & LaGrone, A. H. (1962). Digital computation of the mutual impedance between thin dipoles. *IRE Transactions on Antennas and Propagation*, *10*(2), 172–178. https://doi.org/10.1109/tap.1962.1137835

Balanis, C. A. (2005). *Antenna theory* (3rd edn). Wiley-Interscience.

Best, S. R. (2011). Mutual coupling between orthogonal electrically small dipole antennas. In *European conference on antennas and propagation* (pp. 1663–1666). https://doi.org/10.1109/EuCAP.2012.6206562

Czyz, J. (1957). Impedancje wzajemne w plaskich ukladach antenowych. *Rozprawy Elektrotecltniczne*, *3*(1), 139–166.

Gupta, I., & Ksienski, A. (1983). Effect of mutual coupling on the performance of adaptive arrays. *IEEE Transactions on Antennas and Propagation*, *31*(5), 785–791. https://doi.org/10.1109/tap.1983.1143128

Han, J. H., & Myung, N. H. (2012). Exact and simple calculation of mutual impedance for coplanar-skew dipoles. *Electronics Letters*, *48*(8), 423–425. https://doi.org/10.1049/el.2012.0420

Han, J. H., Song, W. Y., Oh, K. S., & Myung, N. H. (2012). Simple formula and its exact analytic solution of mutual impedance for nonplanar-skew dipoles. *Progress in Electromagnetics Research*, *132*, 551–570. https://doi.org/10.2528/pier12083002

Han, J. H., Song, W. Y., Oh, K. S., & Myung, N. H. (2013). Analytical derivation of mutual impedance between two arbitrarily located and slanted dipoles using effective length vector. In *Asia-pacific microwave conference*.

Huang, Z., Balanis, C. A., & Birtcher, C. R. (2006a). Mutual coupling compensation in UCAs: Simulations and experiment. *IEEE Transactions on Antennas and Propagation*, *54*(11), 3082–3086. https://doi.org/10.1109/TAP.2006.883989

Huang, Z., Balanis, C. A., & Birtcher, C. R. (2006b). Mutual coupling in beamforming with circular array. In *IEEE antennas and propagation society international symposium* (pp. 4785–4788). https://doi.org/10.1109/APS.2006.1711711

Khan, S., & Wong, K. T. (2019). Electrically long dipoles in a crossed pair for closed-form estimation of an incident source's polarization. *IEEE Transactions on Antennas and Propagation*, *67*(8), 5569–5581. https://doi.org/10.1109/tap.2019.2916581

Murray, F. H. (1933). Two skew antenna wires. *Proceedings of the Institute of Radio Engineers*, *21*(1), 154–158. https://doi.org/10.1109/jrproc.1933.227887

Richmond, J. H. (1970). Coupled linear antennas with skew orientation. *IEEE Transactions on Antennas and Propagation*, *18*(5), 694–696. https://doi.org/10.1109/tap.1970.1139751

Richmond, J. H., & Geary, N. H. (1970). Mutual impedance between coplanar-skew dipoles. *IEEE Transactions on Antennas and Propagation*, *18*(3), 414–416. https://doi.org/10.1109/tap.1970.1139705

Richmond, J. H., & Geary, N. H. (1975). Mutual impedance of nonplanar-skew sinusoidal dipoles. *IEEE Transactions on Antennas and Propagation*, *23*(3), 412–414. https://doi.org/10.1109/tap.1975.1141083

Schmidt, K. E. (1996). Simplified mutual impedance of nonplanar skew dipoles. *IEEE Transactions on Antennas and Propagation*, *44*(9). https://doi.org/10.1109/8.535390

Svantesson, T. (1998). The effects of mutual coupling using a linear array of thin dipoles of finite length. In *IEEE signal processing workshop on statistical signal and array processing*.

Svantesson, T. (1999). Modeling and estimation of mutual coupling in a uniform linear array of dipoles. In *IEEE international conference on acoustics, speech, and signal processing* (Vol. 5), (pp. 2961–2964). https://doi.org/10.1109/icassp.1999.761384

Weber, R. J., & Huang, Y. (2012). Performance analysis of direction of arrival estimation with a uniform circular array. In *IEEE aerospace conference*.

Wong, K. T., Song, Y., Fulton, C. J., Khan, S., & Tam, W.-Y. (2017). Electrically "long" dipoles in a collocated/orthogonal triad—for direction finding or polarization estimation. *IEEE Transactions on Antennas and Propagation*, *65*(11), 6057–6067. https://doi.org/10.1109/tap.2017.2748183

Yang, C., & Ruan, Y. Z. (1993). Eigenvalues of covariance matrix of adaptive array with mutual coupling and two correlated sources present. In *IEEE antennas and propagation society international symposium* (pp. 706–709). IEEE.

Yuan, X., Wong, K. T., & Agrawal, K. (2012). Polarization estimation with a dipole-dipole pair, a dipole-loop pair, or a loop-loop pair of various orientations. *IEEE Transactions on Antennas and Propagation*, *60*(5), 2442–2452. https://doi.org/10.1109/tap.2012.2189740